Topographic roughness on forested hillslopes: a theoretical approach for quantifying hillslope sediment flux from tree throw

Tyler H Doane[1], Douglas Arthur Edmonds[2], Brian J Yanites[2], and Quinn W Lewis[3]

[1]Indiana University-Bloomington
[2]Indiana University
[3]University of Waterloo

November 22, 2022

Abstract

Tree uprooting is an observable and consequential process that suddenly moves soil downslope, inverts the soil column, and roughens the surface with pit-mound topography. Quantifying fluxes due to tree throw is complicated by its stochastic nature and estimation requires averaging over a large area or long time. Here, we develop theory that leads to a dimensionless metric directly measurable from high resolution topographic data. The theory explains the flux and topographic roughness as a function of tree throw production and decay rate by creep-like processes. We then form a dimensionless variable that is the ratio of fluxes due to three throw versus creep-like processes. Applying the theory to hillslopes in Southern Indiana, we find that tree throw accounts for 10 to 20\% of the hillslope sediment flux. The theoretical and observational findings provide a framework and important constraints on quantifying Critical Zone function from topographic parameters such as roughness.

Topographic roughness on forested hillslopes: a theoretical approach for quantifying hillslope sediment flux from tree throw

Tyler H. Doane[1], Douglas Edmonds[1], Brian J. Yanites[1], Quinn Lewis [2]

[1]Indiana University-Bloomington, Department of Earth and Atmospheric Sciences, Bloomington, IN, USA
[2]Waterloo University, Department of Geography and Environmental Management, Waterloo, ON, CA

Key Points:

- The expected topographic variance is a function of the ratio of tree throw rates to creep-like diffusivity.
- Tree throw accounts for 10-20% of the hillslope sediment flux in southern Indiana.
- Tree throw occurs more frequently on steep, east facing hillslopes which is consistent with the dominant wind directions.

Corresponding author: Tyler Doane, doanet@iu.edu

Abstract

Tree uprooting is an observable and consequential process that suddenly moves soil downslope, inverts the soil column, and roughens the surface with pit-mound topography. Quantifying fluxes due to tree throw is complicated by its stochastic nature and estimation requires averaging over a large area or long time. Here, we develop theory that leads to a dimensionless metric directly measurable from high resolution topographic data. The theory explains the flux and topographic roughness as a function of tree throw production and decay rate by creep-like processes. We then form a dimensionless variable that is the ratio of fluxes due to three throw versus creep-like processes. Applying the theory to hillslopes in Southern Indiana, we find that tree throw accounts for 10 to 20% of the hillslope sediment flux. The theoretical and observational findings provide a framework and important constraints on quantifying Critical Zone function from topographic parameters such as roughness.

Plain Language Summary

When trees fall on hillslopes, they often uproot a volume of soil that is attached to the roots. Because trees usually fall downslope, this uprooted soil also moves down the hillslope, contributes to erosion, and leaves characteristic pit and mound shapes on the surface. Despite the topographic signature of the process, quantifying how much dirt trees move downslope is complicated by the randomness that drives the process. We develop theory that explains the roughness of hillslope topography and how it relates to sediment transport rates driven by tree throw. We then map topographic roughness over a county in southern Indiana and demonstrate that tree throw accounts for 10 to 20% of the sediment motions on hillslopes. Further, we demonstrate that east facing hillslopes tend to have more tree throw events which coincides with the dominant wind directions and illustrates that extreme wind events drive most tree throw events in southern Indiana.

1 Introduction

The rate and style of sediment transport processes on hillslopes are central to understanding landscape evolution (Roering et al., 2001, 2007), geochemical cycling (Maher, 2010; Yoo et al., 2007; Lebedeva & Brantley, 2013), soil production (Heimsath et al., 2001; Mudd & Furbish, 2004; Gabet & Mudd, 2010; Riebe et al., 2003; Ferrier & Kirchner, 2008), sediment supply to watersheds (Syvitski, 2003), and the dynamics of the Critical Zone (Brantley, McDowell, et al., 2017; Brantley, Eissenstat, et al., 2017). On hillslopes, a suite of processes that include freeze-thaw (Anderson, 2002), wetting-drying (Struck et al., 2018), and bioturbation (Gabet et al., 2003) disturb unconsolidated soil and sediment which leads to bulk downslope creep-like motion (Culling, 1963; Furbish et al., 2009). Observation and quantification of these creep-like processes is often obfuscated by the small scale over which they operate and the slow bulk transport rates that they produce. Tree throw, however, is a sediment transport process that occurs when trees topple and uproot a mass of soil – leaving a clear pit-mound couplet as a topographic signature. In contrast to the suite of creep-like processes, tree throw suddenly moves and mixes soil, which inverts any soil-depth varying chemical or physical properties. Tree throw therefore is a uniquely consequential and measurable process on hillslopes, yet the relative magnitudes of sediment fluxes due to tree throw and creep-like processes remain unknown.

Tree throw has been the subject of many field and numerical studies that quantify the sediment flux, (Gabet et al., 2003; Martin et al., 2013; Phillips et al., 2017; Hancock & Lowry, 2021; Šamonil et al., 2020) or demonstrate the consequences for weathering and soil production (Gallaway et al., 2009; Gabet & Mudd, 2010; Šamonil et al., 2013). Quantifying the sediment flux due to tree throw typically involves measuring the volumes of sediment attached to uprooted trees and constraining event frequency by either dating material deposited beneath mounds (Schaetzl & Follmer, 1990; Šamonil et al., 2013) or by tree census (Gallaway et al., 2009; Martin et al., 2013; Šamonil et al., 2020). However, tree throw is often caused by rare extreme wind events that impart a drag force on the canopy which exceed a resisting force of the soil. Such events occur with a large range of magnitudes and the recurrence intervals for large events can be on the order of decades (Gallaway et al., 2009; Hancock & Lowry, 2021). Therefore, quantification of tree throw by direct human observation is beyond our capabilities and requires that we average over the full range of the process. This requires either a very long record through time or very large domain that samples a great number of tree throw events. The land surface is a faithful record of past tree throw events as it accumulates pit-mound couplets through time and the topographic roughness of a surface reflects a long record of tree throw events.

In this paper, we develop theory for the expected topographic roughness (quantified by the topographic variance) of a hillslope for a given frequency of tree throw events

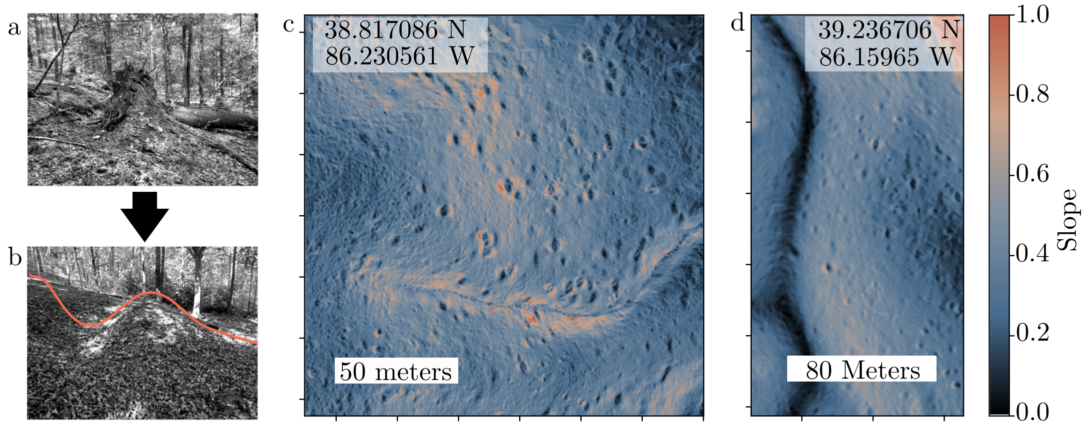

Figure 1. (A) Image of a tree throw root ball and (B) the subsequent transition to a characteristic pit-mound couplet. On many hillslopes in southern Indiana pit-mound couplets are the primary roughness features which creates the pocked texture. This texture is visible from (C) 0.25 m and (D) 0.76 m resolution digital elevation models. Hatch marks on the images are equal intervals of meters.

and magnitude of topographic smoothing from creep-like processes. We then leverage the theory to form a dimensionless variable that is composed entirely of measurable topographic variables and is the ratio of the hillslope sediment flux due to tree throw versus all creep-like processes. Topographic roughness created by tree throw is observable in high resolution topographic data and the theory may be applied across large areas. We apply the theory to 1,910 hillslopes selected from over 800 km^2 in southern Indiana (Brown County) to obtain estimates of the percentage of the flux due to tree throw. We demonstrate that tree throw accounts for approximately 10-20% of the hillslope sediment flux and highlight an aspect-dependency that is consistent with dominant wind directions in southern Indiana.

2 Theory

Here we construct the ratio of sediment flux due to tree throw versus creep-like processes. We develop analytical expressions for the flux due to tree throw and the expected topographic variance that reflects the balance between roughness production by tree throw and roughness erasure by creep-like processes. These two components are then combined to form the desired ratio of volumetric fluxes.

2.1 Flux due to tree throw

Previous work quantifies the flux due to tree throw as the product of the frequency of the process and the volume that it mobilizes, which can be measured from the volumes of either pits or uprooted sediment attached to roots (Gabet et al., 2003; Gallaway et al., 2009; Hellmer et al., 2015; Phillips et al., 2017). We present a similar formulation, but cast it in probabilistic terms for particle travel distances. The mean flux for any process is (Furbish & Haff, 2010; Doane et al., 2018)

$$\bar{q}(x,y) = E(x,y)\mu_r(x,y) \tag{1}$$

where E [$\mathrm{L}^3\ \mathrm{L}^{-2}\mathrm{T}^{-1}$] is a volumetric entrainment rate and μ_r is the mean travel distance. E involves the frequency of tree throw events per unit area and the volume of root balls, which is a stochastic and noise-driven component that is not directly measurable over short timescales or small spatial scales. In contrast, particle travel distances relate directly to the geometry of pit-mound couplets (Figure 2).

We define an initial couplet geometry that is an approximation to those observed in nature (Figure 2),

$$\zeta'(x,y) = \frac{2Ax}{l^2} e^{-\left(\frac{x^2}{l^2}+\frac{y^2}{w^2}\right)}\ , \tag{2}$$

where ζ' [L] is the land-surface elevation, x and y [L] are horizontal positions, A [L^2] is a squared amplitude, and l and w are characteristic length scales. Note that (2) is a Gaussian in the y-direction and a derivative of a Gaussian in the x-direction. Previous work has suggested alternative forms (two anti-symmetric semi-spheres) for the initial condition of pit-mound couplets (Gabet et al., 2003; Gabet & Mudd, 2010; Martin et al., 2013; Šamonil et al., 2020); however, we prefer this formulation as it approximates natural couplet geometries and is mathematically simple to work with. The form of (2) represents the initial condition of pit-mound couplets once the tree roots have rotted away (5-10 years after the tree topples in temperate environments (Schaetzl & Follmer, 1990)) so that the couplet may evolve by creep-like processes. With this definition of the initial condition, the 'throw' component involves the tree toppling and the decay of roots which drops particles and constructs smooth pit-mound couplets. Based on (1), (2), and using the idealized geometry of couplets and allowing for A and l to be random variables, we find that the average flux due to tree throw on a hillslope is (Appendix A),

$$q_{TT}(x,y) = p(x,y)\frac{\sqrt{2}\pi\mu_A\left(\mu_l^2+\sigma_l^2\right)}{\phi}\ , \tag{3}$$

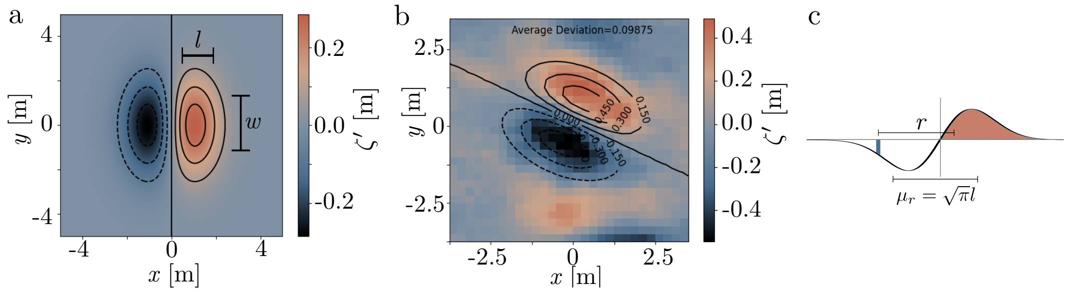

Figure 2. (a) Two dimensional view of an idealized pit-mound couplet. (b) Comparison of idealized and natural pit-mound couplet illustrating good agreement. (c) Conceptual diagram illustrating how we calculate the probability function of travel distances, r. l and w are characterisic length scales of pit-mound couplets and μ_r is the mean particle travel distance.

where μ_X and σ_X^2 refer to the mean and variance of variable X, and we have introduced $\phi = l/w$ because we expect l and w to co-vary on a given slope. The production rate, p [L^{-2} T^{-1}], is the only variable that is not directly measurable from topography.

The idealized pit-mound geometry should vary with slope. When trees fall on progressively steeper slopes, more of the uprooted sediment moves further downslope, which increases l and ϕ (Gabet et al., 2003). To account for this we numerically simulate a one-dimensional model of pit-mound formation on different slopes which suggests $l \approx 1 + S$ where S is land-surface slope (S4). We note that equation (3) assumes that all trees fall directly downslope but, in nature, trees can fall in all directions. However, observations of tree throw resulting from ice storms demonstrates that trees typically fall downslope (Hellmer et al., 2015), which indicates that they tend to have weaker resiting forces in the downslope direction. Most pit-mound couplets are oriented along hillslope contours in southern Indiana, suggesting that downslope transport is the dominant mode of tree throw in this setting.

2.2 Topographic Roughness

Tree throw is the only geomorphic process we know of that adds topographic roughness to soil mantled and forested hillslopes at the scale of meters. Topographic roughness can be quantified with the average concavity (Booth et al., 2017; LaHusen et al., 2016), fitted polynomial functions (Milodowski et al., 2015), and the standard deviation or variance of detrended topography (Roth et al., 2020). We use the topographic variance to quantify roughness because we can derive an analytical solution for the expected variance that reflects the balance between tree throw frequency and the pace of couplet degradation by creep-like processes.

Couplets degrade by the action of all creep-like processes which drive the creation and collapse of porosity. When the land-surface is inclined, this leads to downslope sediment motion at a rate that scales with slope (Furbish et al., 2009). A linear model for creep-like processes has a long legacy in geomorphology (Culling, 1963),

$$q_c = -D\nabla\zeta \,, \tag{4}$$

where q_c [L^2 T^{-1}] is the volumetric flux, D [L^2 T^{-1}] is a topographic diffusivity, and ζ is the land-surface elevation. Placing (4) into the Exner equation leads to the linear diffusion equation for the evolution of topography (Fernandes & Dietrich, 1997; Furbish & Fagherazzi, 2001; Richardson et al., 2019),

$$\frac{\partial\zeta}{\partial t} = D\nabla^2\zeta \,. \tag{5}$$

We note that nonlinear slope- (Roering et al., 2001) and soil thickness-dependent (Furbish et al., 2009; Mudd & Furbish, 2004; Johnstone & Hilley, 2015) formulations are alternative flux models. However, neither of these models leads to a significant difference in the evolution of topographic variance for pit-mound couplets (S2) so we only consider linear diffusion here.

We solve the diffusion equation for topography with an initial condition represented by (2) to understand the temporal evolution of the topographic variance of a single pit-mound couplet. To do so, we transform the problem into the wavenumber domain via the Fourier Transform and apply Parseval's Theorem, which states that the integral of the square of Fourier Transform amplitudes is equal to the integral of the square of the signal in the arithmetic domain (Appendix B). The sum of squares equals the sample variance when one divides by the size of the domain so these two steps lead to an analytical solution for the time evolution of topographic variance of a pit-mound couplet. The topographic variance of an entire hillslope is the integral of all couplets of all ages, which amounts to a convolution of tree throw production and decay rates,

$$\sigma_\zeta^2(t) = \frac{A^2 w^2 l^2 \pi}{32} \int_{-\infty}^{t} p(t') \left[\frac{l^2}{4} + D[t-t']\right]^{-3/2} \left[\frac{w^2}{4} + D[t-t']\right]^{-1/2} \mathrm{d}t' \,, \tag{6}$$

where t' is an earlier time and $t-t'$ is a couplet age. Given a time-series of tree throw production rates, (6) describes the topographic variance at any moment. The produc-

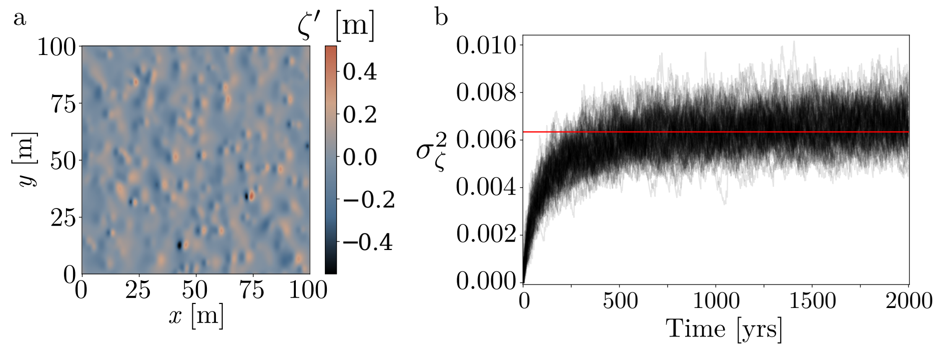

Figure 3. a) A rough surface that is the result of a numerical simulation with $D = 0.005$ and a mean production rate of one tree per year per 10,000 m^2. b) The time series of one hundred numerical simulations with the same parameters (gray) and the expected variance (red).

tion rate of tree throw will be some noisy signal through time and so too is the time series of topographic variance. For the purpose of this paper, we consider the expected topographic variance, which only involves the mean production rate, μ_p. Performing the integration in (6) (over all couplets of all ages) yields the expected topographic variance

$$\mathrm{E}(\sigma_\zeta^2) = \frac{\mu_p A^2 l^2 \pi}{4D(\phi^2 + \phi)}\,. \tag{7}$$

If we allow for A and l to be random variables with finite covariance, then the expected topographic variance is

$$\mathrm{E}(\sigma_\zeta^2) = \frac{\mu_p \left(\left(\mu_A^2 + \sigma_A^2\right)\left(\mu_l^2 + \sigma_l^2\right) + \mathrm{cov}(A^2, L^2)\right)\pi}{4D\left(\phi^2 + \phi\right)}\,. \tag{8}$$

We numerically test this result by simulating random production and diffusion (equation 5) of pit-mound couplets on a flat surface. For each one year time step, a number of new pit-mound couplets is selected from an exponential distribution of production rates. The exponential distribution reflects our intuition that at a single hillslope and in most years, zero to few tree throw events will occur and there will be rare years with many tree throw events. The model then populates a two-dimensional domain with new pit-mound couplets with parameters that are chosen from distributions that have a small but finite amount of covariance. Roughness on the numerical surface initially increases until it reaches a steady state value which it oscillates around and coincides with (8) (Figure 3).

Although (8) accurately predicts the expected topographic variance of the numerical model, it contains two unknown rate constants, μ_p and D. Previous efforts attempt to understand values of D from a statistical mechanics (Furbish et al., 2009) or empirical perspective (Richardson et al., 2019). However, identifying the value of D for a particular landscape remains a challenge and is a source of uncertainty. There are also estimates of tree throw production rates (Schaetzl et al., 1990; Phillips et al., 2017; Šamonil et al., 2020), but the stochasticity of tree throw over timescales of decades to centuries limits the constraints of μ_p.

Equation 8 demonstrates that rougher hillslopes reflect a relatively high tree throw production rate and low diffusivity. Although we cannot know μ_p and D apriori, we can learn about the relative magnitude of the sediment fluxes due to tree throw and creep-like processes. First, we rewrite the expression for q_{TT} by rearranging (8) to solve for μ_p. This places σ_ζ^2 and D in the numerator of (3). Forming the ratio then leads to,

$$R = \frac{q_{TT}}{q_c} = 4\sqrt{2}\frac{\mu_A\,(\phi+1)}{(\mu_A^2+\sigma_A^2)}\frac{\sigma_\zeta^2}{|S|}\,, \tag{9}$$

where we have assumed that $\mathrm{cov}(A^2, L^2)$ is negligible (S3). Note that all parts of (9) are measurable from high resolution topographic data. We now turn to calculations of R by measuring σ_ζ^2, $|S|$, and parameterization of A and ϕ in a forested landscape.

3 Measuring topographic variance and R with high-resolution topography

3.1 Constraining pit-mound geometry

We parameterize A, l, and ϕ by fitting the idealized couplet geometry to pit-mound couplets that are clearly visible in high resolution topography. We fit 101 pit-mound couplets from 0.25 m resolution, drone-collected lidar (S1). Couplets that we identify from lidar are likely to vary in age and therefore may have partially diffused. The shape $A/(wl)$ of each pit-mound couplet is a proxy for age, and the youngest will have the largest value of this ratio (i.e. tall and narrow). We select the 50 freshest/youngest based on this metric and extract values for $\mu_A = 0.68$, $\sigma_A^2 = 0.05$, $\phi = 0.83$, and $\mathrm{Cov}(A^2, L^2) = 0.005$ (S3). The covariance and variance terms are negligible relative to the average values and so they may be dropped from (8)

3.2 Measuring Topographic Variance

We used a 2017 lidar survey of Indiana collected via the USGS 3D elevation program, that produced digital elevation models (DEMs) at 0.76 m resolution to measure topographic variance. We emphasize that 0.76 m resolution DEMs are capable of capturing the majority of topographic variance from tree throw (S1). We focus our study on Brown County, which is a rural county in south-central Indiana with moderate relief (200 meters) and locally steep slopes (up to ≈ 1). The Borden Group, a Missippian siltstone interbedded with limestone, underlies the entire county (Thompson & Sowder, 2005). Brown County is south of the southern terminus of the last glacial extent and the topography lacks glacial roughness features like hummocky topography or glacial erratics so that hillslope roughness is reliably created by tree throw.

We manually define 1,910 forested hillslopes in Brown County that are minimally dissected by first-order gullies. We first run a high-pass filter over 1.5x1.5 km sections of the land surface with a Gaussian filter with a length scale of 3.8 meters (5 pixels) to filter out hillslope- and valley-scale topography. The high pass filter highlights a number of roughness features including pit-mound couplets, channel banks, geologic contacts, and infrastructure. We manually exclude hillslopes with these other roughness features. For each area of interest, we calculate the topographic roughness as the variance of the high pass filter output.

4 Results

Measurements of topographic variance for 1910 hillslopes from Brown county (Figure 4a) span over an order of magnitude from 0.001 up to 0.03. There is a modest positive relationship between topographic variance and slope (Figure 4b). However, the spread of measured variance values also increases with slope. Topographic variance also depends on slope aspect (Figure 4c) with northeast facing slopes having the largest measured values and west-facing slopes having the lowest. We observe the same trend in the distribution of average slopes of the hillslopes that we selected with east-facing slopes generally being steeper than west facing slopes (Figure 4d). The reason for the slope-magnitude sampling discrepancy between east and west slopes is that there is an aspect-dependent drainage density in which first order channels and gullies tend to dissect steep west facing slopes more frequently than steep east facing slopes. This limits our ability to sample steep west facing slopes as channelization processes overprint the hillslopes.

Sediment flux due to tree throw increases by roughly 50% on east facing slopes (Figure 4f). The average values of R (calculated by weighting hillslopes by area) vary from

0.12 to 0.22 on west- and east-facing slopes respectively (Figure 4e), accounting for $q_{TT}/(q_c + q_{TT}) = 11\%$ and 18% of the hillslope sediment flux on those slopes. Several thousand eddy covariance measurements of wind velocity from a nearby AmeriFlux tower demonstrate that wind blows most frequently to the northeast and least frequently to the west (Novick & Phillips, 2020) suggesting that the larger R and variance on east-facing hillslopes is caused by wind-blown tree throw as opposed to trees aging or snow loading.

The spread in R values (Figure 4e) should not be interpreted as a range of tree throw frequency because it reflects the stochastic nature of tree throw. Only the average value of R is meaningful. By sampling 1910 hillslopes across Brown County, we attempt to exchange space for time so that for each primary direction, we have sampled values that approach the full range of natural topographic roughness and the average sample roughness is approximately equal to the expected roughness for a given population of hillslopes (e.g. east vs west).

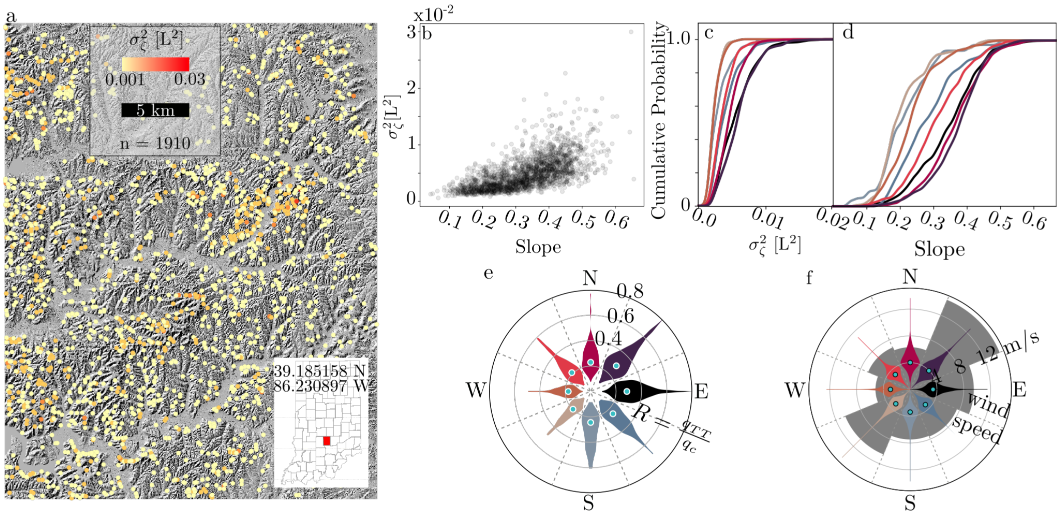

Figure 4. a) Hillshade of Brown County, IN with points of selected hillslopes colored by the measured topographic variance. b) Topographic variance as a function of slope. Cumulative probability plots of measured topographic variance (c) and slope (d) colored by aspect. e) Rose diagram of violin plots for R illustrating a modest aspect dependency. f) Rose diagram of wind speeds (colors) and relative frequencies (gray).

5 Discussion and Conclusions

We have developed theory that explains the topographic roughness of forested hillslopes and a tool that maps the relative contributions to the volumetric sediment flux from tree throw and creep-like processes. The topographic variance of a hillslope at any moment is a convolution of a noisy signal through time that depends on the stochastic occurrence of tree throw events and their decay due to creep-like processes. This leads to a noisy signal of topographic roughness that oscillates around an expected value. In general, greater average frequency of tree throw occurrences per area per time and lower values for diffusivity lead to rougher hillslopes (e.g. the p/D term in Equation 8). This is the first theory to address topographic roughness due to tree throw of forest floors and is key for developing methods for quantifying tree throw.

Our theory assumes that at the scale of meters, pit-mound couplets are the primary roughness feature on hillslopes. Temperate, moderate relief, forested hillslopes lack other sources of roughness such as gopher mounds (Jyotsna & Haff, 1997), sediment mounds that form under shrubs (Worman & Furbish, 2019) (semi-arid), landslides (LaHusen et al., 2016; Booth et al., 2017) and their scarps (steeplands), and solifluction lobes (Glade et al., 2021) (periglacial). Fossorial mammals either produce topographic roughness that are too small (e.g. mole hills) or far too rare (e.g. bear burrows) to explain the observed meter scale roughness in these landscapes. Lithologic contacts in such landscapes are localized and affect few hillslopes. Creep-like processes unconditionally smooth topography (Furbish & Fagherazzi, 2001) so in forested settings we are confident that the topographic roughness in this setting is primarily driven by the production and decay of tree throw couplets.

We have developed a topographic variable, R, to describe the relative fluxes due to roughening processes (i.e. tree throw) and smoothing processes (e.g. creep). R is directly measurable from topography and allows for widespread quantification of a process that is driven by stochastic events that occur with frequencies that frustrate direct human observation. The roughness of the land-surface is a record of all past events over timescales of decades to centuries which is required for measuring the contribution to the flux for tree throw. In southern Indiana, R indicates that tree throw accounts for roughly 11% to 18% of volumetric sediment flux.

Despite the clearly rough hillslopes of southern Indiana, 11 to 18% represents a somewhat modest contribution to the total hillslope sediment flux. However, we suggest that tree throw is unlikely to contribute a majority of the volumetric sediment flux for several reasons. First, because soil is an unconsolidated medium, creep will always occur (Ferdowsi et al., 2018; Deshpande et al., 2021) and tree throw can never account for all of the volumetric flux. Second, although rough hillslopes are common in southern Indiana and are clearly observable, there are many more smooth and moderately rough hillslopes (Figure 4b,c,e) that dominate the landscape. Third, tree throw is limited by population dynamics (Gallaway et al., 2009; Gabet & Mudd, 2010) which sets the spacing of trees, recruitment of new saplings, and growth rates. All of these may amount to an upper limit of R being around what we have measured in southern Indiana. However, further measurement of R in other settings are required to more definitively quantify the limits of tree throw.

Despite the relatively small contributions to the volumetric flux, tree throw is a unique hillslope transport process that may have an outsized role in influencing Critical Zone processes. Tree throw episodically and suddenly creates topographic roughness, inverts the soil column, and has the potential to expose fresh bedrock. Each of these has potential implications to affect hydrologic pathways (Phillips et al., 2017)), soil development (Šamonil et al., 2020), chemical weathering, and soil production rates (Gabet & Mudd, 2010). We anticipate that R will be a valuable tool that is readily available for quantifying the magnitude and frequency of tree throw and its impact on the Critical Zone.

Appendix A Mean Travel Distance

We calculate the mean travel distance by assuming that a particle may be entrained/deposited from any location within the pit/mound. The pit and mound individually have a morphology that resembles a Rayleigh distribution,

$$f_z(z) = \frac{2z}{\omega^2} e^{-\frac{z^2}{\omega^2}} \tag{A1}$$

where z is the random variable and ω is a parameter. The mean of a Rayleigh distribution is

$$\mu_r = \frac{\sqrt{\pi}}{2} l\,. \tag{A2}$$

The total travel distance is the difference between the mean deposition location and mean entrainment location,

$$\mu_r(r) = \sqrt{\pi} l\,. \tag{A3}$$

The volumetric entrainment rate, is the volume of the pit multiplied by a production rate, p [L^{-2}],

$$E(x,y) = p(x,y)\sqrt{\pi} l \int_{-\infty}^{\infty}\int_{-\infty}^{0} -\frac{2Ax}{l^2} e^{\left(-\frac{x^2}{l^2}\frac{y^2}{w^2}\right)} \mathrm{d}x\mathrm{d}y = p(x,y)\sqrt{2\pi} Awl\,. \tag{A4}$$

Equations (A3) and (A4) combine to form (3).

Appendix B Topographic Variance

The Fourier transform of (1) is

$$\hat{\zeta}(k_x, k_y) = -4iAwlk_x\pi e^{-\frac{k_x^2 l^2}{4} - \frac{k_y^2 w^2}{4}}\,, \tag{B1}$$

where k_x and k_y is the wavenumber [L^{-1}] (radians per unit length) in the x and y directions. The analytical solution for the diffusion of a couplet through time in wavenumber domain (B1) is

$$\hat{\zeta}(k_x, k_y, t) = -4iAwlk_x\pi e^{-k_x^2\left(Dt+\frac{l^2}{4}\right) - k_y^2\left(Dt+\frac{w^2}{4}\right)} \tag{B2}$$

where t [T] is age of the couplet. Parseval's Theorem states that the integral of the squared amplitudes of a Fourier transform equals the sum of squares of the original signal. Roughness has a mean of zero, so in this case Parseval's Theorem is directly related to topographic variance and we obtain a time-evolution of topographic variance of a single pit-mound couplet. This step yields,

$$\sigma_\zeta^2(t) = \frac{1}{4\pi^2 H}\int_{-\infty}^{\infty}\int_{-\infty}^{\infty} |\hat{\zeta}(k_x, k_y, t)|^2 \mathrm{d}k_x \mathrm{d}k_y = \frac{A^2 w^2 l^2 \pi}{32H}\left(\frac{l^2}{4} + Dt\right)^{-3/2}\left(\frac{w^2}{4} + Dt\right)^{-1/2}, \tag{B3}$$

where H [L^2] is the area of the domain. The topographic variance of an entire hillslope is the integral over all couplets of all ages which is presented in (6). Note that the production rate, p has units (L^{-2} T^{-1}) so that H is now included in p.

Acknowledgments

Data and Python scripts used to generate data are available at https://github.com/tdoane/Topographic-Variance/ and will be available in a maintained in the IUScholarWorks repository upon publication (https://openscholarship.indiana.edu/data-deposit). This project was supported by the Environmental Resilience Institute, funded by Indiana Universitys Prepared for Environmental Change Grand Challenge initiative.

References

Anderson, R. S. (2002). Modeling the tor-dotted crests, bedrock edges, and parabolic profiles of high alpine surfaces of the Wind River Range, Wyoming. *Geomorphology*, *46*(1-2), 35–58. doi: 10.1016/S0169-555X(02)00053-3

Booth, A. M., LaHusen, S. R., Duvall, A. R., & Montgomery, D. R. (2017). Holocene history of deep-seated landsliding in the north fork stillaguamish river valley from surface roughness analysis, radiocarbon dating, and numerical landscape evolution modeling. *Journal of Geophysical Research: Earth Surface*, *122*(2), 456–472. doi: 10.1002/2016JF003934

Brantley, S. L., Eissenstat, D. M., Marshall, J. A., Godsey, S. E., Balogh-Brunstad, Z., Karwan, D. L., ... Weathers, K. C. (2017). Reviews and syntheses: on the roles trees play in building and plumbing the critical zone. *Biogeosciences*, *14*(22), 5115–5142. doi: 10.5194/bg-14-5115-2017

Brantley, S. L., McDowell, W. H., Dietrich, W. E., White, T. S., Kumar, P., Anderson, S. P., ... Gaillardet, J. (2017). Designing a network of critical zone observatories to explore the living skin of the terrestrial Earth. *Earth Surface Dynamics*, *5*(4), 841–860. doi: 10.5194/esurf-5-841-2017

Culling, W. E. H. (1963). Soil creep and the development of hillside slopes. *The Journal of Geology*, *71*(2), 127–161. (ISBN: 0022-1376 Publisher: University of Chicago Press)

Deshpande, N., Furbish, D., Arratia, P., & Jerolmack, D. (2021). The fragility of creeping hillslopes. *Nature Communications*, *12*(3909). doi: 10.1038/s41467-021-23979-z

Doane, T. H., Furbish, D. J., Roering, J. J., Schumer, R., & Morgan, D. J. (2018). Nonlocal sediment transport on steep lateral moraines, eastern Sierra Nevada, California, USA. *Journal of Geophysical Research: Earth Surface*, *123*(1), 187–208. doi: 10.1002/2017JF004325

Ferdowsi, B., Ortiz, C. P., & Jerolmack, D. J. (2018). Glassy dynamics of landscape evolution. *Proceedings of the National Academy of Sciences*, *115*(19), 4827–4832. doi: 10.1073/pnas.1715250115

Fernandes, N. F., & Dietrich, W. E. (1997). Hillslope evolution by diffusive processes: The timescale for equilibrium adjustments. *Water Resources Research*, *33*(6), 1307–1318. doi: 10.1029/97WR00534

Ferrier, K. L., & Kirchner, J. W. (2008, August). Effects of physical erosion on chemical denudation rates: A numerical modeling study of soil-mantled hillslopes. *Earth and Planetary Science Letters*, *272*(3-4), 591–599. doi: 10.1016/j.epsl.2008.05.024

Furbish, D. J., & Fagherazzi, S. (2001). Stability of creeping soil and implications for hillslope evolution. *Water Resources Research*, *37*(10), 2607–2618. doi: 10.1029/2001WR000239

Furbish, D. J., & Haff, P. K. (2010). From divots to swales: Hillslope sediment transport across divers length scales. *Journal of Geophysical Research: Earth Surface*, *115*(F3). doi: 10.1029/2009JF001576

Furbish, D. J., Haff, P. K., Dietrich, W. E., & Heimsath, A. M. (2009). Statistical description of slope-dependent soil transport and the diffusion-like coefficient. *Journal of Geophysical Research*, *114*, F00A05. doi: 10.1029/2009JF001267

Gabet, E. J., & Mudd, S. M. (2010). Bedrock erosion by root fracture and tree throw: A coupled biogeomorphic model to explore the humped soil production function and the persistence of hillslope soils. *Journal of Geophysical Research: Earth Surface*, *115*(F4). (Publisher: Wiley Online Library)

Gabet, E. J., Reichman, O. J., & Seabloom, E. W. (2003). The effects of bioturbation on soil processes and sediment transport. *Annual Review of Earth and Planetary Sciences*, *31*(1), 249–273. doi: 10.1146/annurev.earth.31.100901.141314

Gallaway, J. M., Martin, Y. E., & Johnson, E. A. (2009). Sediment transport due to tree root throw: integrating tree population dynamics, wildfire and geomorphic response. *Earth Surface Processes and Landforms*, *34*(9), 1255–1269. doi: 10.1002/esp.1813

Glade, R. C., Fratkin, M. M., Pouragha, M., Seiphoori, A., & Rowland, J. C. (2021). Arctic soil patterns analogous to fluid instabilities. *Proceedings of the National Academy of Sciences*, *118*(21). doi: 10.1073/pnas.2101255118

Hancock, G., & Lowry, J. (2021). Quantifying the influence of rainfall, vegetation and animals on soil erosion and hillslope connectivity in the monsoonal tropics of northern australia. *Earth Surface Processes and Landforms*.

Heimsath, A. M., Dietrich, W. E., Nishiizumi, K., & Finkel, R. C. (2001). Stochastic processes of soil production and transport: erosion rates, topographic variation and cosmogenic nuclides in the Oregon Coast Range. *Earth Surface Processes and Landforms*, *26*(5), 531–552. doi: 10.1002/esp.209

Hellmer, M. C., Rios, B. A., Ouimet, W. B., & Sibley, T. R. (2015). Ice storms, tree throw, and hillslope sediment transport in northern hardwood forests. *Earth Surface Processes and Landforms*, *40*(7), 901–912. doi: 10.1002/esp.3690

Johnstone, S. A., & Hilley, G. E. (2015). Lithologic control on the form of soil-mantled hillslopes. *Geology*, *43*(1), 83–86. doi: 10.1130/G36052.1

Jyotsna, R., & Haff, P. K. (1997). Microtopography as an indicator of modern hillslope diffusivity in arid terrain. *Geology*, *25*(8), 695–698. doi: 10.1130/0091-7613(1997)025⟨0695:MAAIOM⟩2.3.CO;2

LaHusen, S. R., Duvall, A. R., Booth, A. M., & Montgomery, D. R. (2016). Surface roughness dating of long-runout landslides near oso, washington (usa), reveals persistent postglacial hillslope instability. *Geology*, *44*(2), 111–114. doi: 10.1130/G37267.1

Lebedeva, M. I., & Brantley, S. L. (2013). Exploring geochemical controls on weathering and erosion of convex hillslopes: beyond the empirical regolith production function. *Earth Surface Processes and Landforms*, *38*(15), 1793–1807. doi: 10.1002/esp.3424

Maher, K. (2010). The dependence of chemical weathering rates on fluid residence time. *Earth and Planetary Science Letters*, *294*(1-2), 101–110. doi: 10.1016/j.epsl.2010.03.010

Martin, Y., Johnson, E., & Chaikina, O. (2013). Interplay between field observations and numerical modeling to understand temporal pulsing of tree root throw processes, canadian rockies, canada. *Geomorphology*, *200*, 89–105. doi: 10.1016/j.geomorph.2013.04.017

Milodowski, D. T., Mudd, S. M., & Mitchard, E. T. A. (2015). Topographic roughness as a signature of the emergence of bedrock in eroding landscapes. *Earth Surface Dynamics*, *3*(4), 483–499. doi: 10.5194/esurf-3-483-2015

Mudd, S. M., & Furbish, D. J. (2004). Influence of chemical denudation on hillslope morphology: INFLUENCE OF CHEMICAL DENUDATION ON HILLSLOPES. *Journal of Geophysical Research: Earth Surface*, *109*(F2). doi: 10.1029/2003JF000087

Novick, K., & Phillips, R. (2020). *Ameriflux us-mms morgan monroe state forest* (No. 18-5). AmeriFlux AMP. doi: 10.17190/AMF/1246080

Phillips, J. D., Šamonil, P., Pawlik, l., Trochta, J., & Daněk, P. (2017). Domination of hillslope denudation by tree uprooting in an old-growth forest. *Geomorphology*, *276*, 27–36. doi: 10.1016/j.geomorph.2016.10.006

Richardson, P. W., Perron, J. T., & Schurr, N. D. (2019). Influences of climate and life on hillslope sediment transport. *Geology*, *47*(5), 423–426. (Publisher: GeoScienceWorld)

Riebe, C. S., Kirchner, J. W., & Finkel, R. C. (2003). Long-term rates of chemical weathering and physical erosion from cosmogenic nuclides and geochemical mass balance. *Geochimica et Cosmochimica Acta*, *67*(22), 4411–4427. doi: 10.1016/S0016-7037(03)00382-X

Roering, J. J., Kirchner, J. W., & Dietrich, W. E. (2001). Hillslope evolution by nonlinear, slope-dependent transport: Steady state morphology and equilibrium adjustment timescales. *Journal of Geophysical Research: Solid Earth*, *106*(B8), 16499–16513. doi: 10.1029/2001JB000323

Roering, J. J., Perron, J. T., & Kirchner, J. W. (2007). Functional relationships between denudation and hillslope form and relief. *Earth and Planetary Science Letters*, *264*(1-2), 245–258. doi: 10.1016/j.epsl.2007.09.035

Roth, D. L., Doane, T. H., Roering, J. J., Furbish, D. J., & Zettler-Mann, A. (2020). Particle motion on burned and vegetated hillslopes. *Proceedings of the National Academy of Sciences*, *117*(41), 25335–25343. doi: 10.1073/pnas.1922495117

Schaetzl, R. J., Burns, S. F., Small, T. W., & Johnson, D. L. (1990). Tree uprooting: Review of types and patterns of soil disturbance. *Physical Geography*, *11*(3), 277–291. doi: 10.1080/02723646.1990.10642407

Schaetzl, R. J., & Follmer, L. R. (1990). Longevity of treethrow microtopography: implications for mass wasting. *Geomorphology*, *3*(2), 113–123. doi: 10.1016/0169-555X(90)90040-W

Struck, M., Jansen, J. D., Fujioka, T., Codilean, A. T., Fink, D., Egholm, D. L., . . .

Kotevski, S. (2018). Soil production and transport on postorogenic desert hillslopes quantified with 10Be and 26Al. *GSA Bulletin*, *130*(5-6), 1017–1040. doi: 10.1130/B31767.1

Syvitski, J. P. (2003). Supply and flux of sediment along hydrological pathways: research for the 21st century. *Global and Planetary Change*, *39*(1-2), 1–11. doi: 10.1016/S0921-8181(03)00008-0

Thompson, T., & Sowder, K. (2005). *Map showing surficial and bedrock geology of indiana* (No. Open-File Study 05-01).

Šamonil, P., Egli, M., Steinert, T., Norton, K., Abiven, S., Daněk, P., ... Tikhomirov, D. (2020). Soil denudation rates in an old-growth mountain temperate forest driven by tree uprooting dynamics, central europe. *Land Degradation & Development*, *31*(2), 222–239.

Šamonil, P., Schaetzl, R., Valtera, M., Goli, V., Baldrian, P., Vakov, I., ... Hort, L. (2013). Crossdating of disturbances by tree uprooting: Can treethrow microtopography persist for 6000years? *Forest Ecology and Management*, *307*, 123–135. doi: 10.1016/j.foreco.2013.06.045

Worman, S. L., & Furbish, D. J. (2019). A probabilistic, biologically informed model of desert shrub population dynamics with the granularity appropriate for geomorphic simulations. *Earth Surface Processes and Landforms*, *44*(6), 1221–1232. doi: 10.1002/esp.4568

Yoo, K., Amundson, R., Heimsath, A. M., Dietrich, W. E., & Brimhall, G. H. (2007). Integration of geochemical mass balance with sediment transport to calculate rates of soil chemical weathering and transport on hillslopes. *Journal of Geophysical Research*, *112*(F2), F02013. doi: 10.1029/2005JF000402

Supporting Information for *Topographic roughness on forested hillslopes: a theoretical approach for quantifying hillslope sediment flux from tree throw*

Tyler H. Doane[1], Douglas A. Edmonds[1], Brian J. Yanites[1], Quinn W. Lewis [2]

[1]Indiana University-Bloomington, Bloomington, IN, USA

[2]Waterloo University, Waterloo, ON, Canada

Tyler H. Doane[doanet@iu.edu]

Contents of this file

1. Text S1 to S4
2. Figures S1 to S4
3. Tables S1

Introduction Here we provide supplemental information that supports the results presented in the main text. We address several items. First, we consider the role that DEM resolution plays. We compare measurements of topographic variance of the same hillslope from two different data sources and demonstrate that, so long as a DEM has a resolution less than a meter that it captures the majority of topographic variance. Second, we demonstrate that different flux models do not result in a meaningful difference in the evolution of topographic variance of a single pit-mound couplet. Therefore, the results do not strongly depend on the choice of flux model. Third, we explain how we parameterized natural pit-mound couplets using high resolution topographic data. Fourth, we consider how initial pit-mound couplet geometry will vary on increasingly sloped terrain. On steeper slopes, more sediment is 'thrown' downslope and l increases. We present results from a simple numerical exercise which demonstrates that l increases linearly with land-surface slope. Last, we present a table of measured R values for 8 directions and the number of measurements in each direction.

1. Resolution We note that the measured topographic variance may differ between the 0.76 m and 0.25m resolution datasets. We anticipate that the finer resolution is closer to the actual resolution, however, we also anticipate that the difference between them is relatively small and does not alter the quantification of tree throw. To demonstrate this, measurements of topographic variance of a single hillslope on private property in Washington County demonstrates similar estimates of the topographic variance whether it is calculated using 0.25 m or 0.76 m-resolution topographic data. On a single hillslope, the measured topographic variance on 0.76 m and 0.25 m resolution topographic data are 0.012 and 0.014 m^2. We are confident that the 0.76 m resolution data is capable of capturing a clear majority of the topographic variance at the meter scale. Lidar data for the high resolution DEM from Washington County was collected by a drone in December 2018. Data collection and processing are outlined in (Lewis et al., 2020).

2. Flux Models We have developed and demonstrated a theory for topographic roughness of forest floors that casts the expected topographic roughness in terms of the rate of tree throw production and the rate of topographic degradation by linear diffusion which is driven by creep-like processes. There are alternatives to linear diffusion to describe topographic evolution, namely nonlinear (Roering et al., 2001, 2007) and soil thickness (Furbish et al., 2009; Mudd & Furbish, 2004) dependent models. The nonlinear model (CITE Roering et al., 1999) is widely used and states that the flux increases nonlinearly with land-surface slope until a critical gradient,

$$q_c = -D_{cn} \frac{\nabla \zeta}{1 - \left(\frac{|\nabla \zeta|}{S_c}\right)^2}, \tag{1}$$

where D_n [L^2 T^{-1}] is a topographic diffusivity and S_c is a critical slope above which the flux is unbound. A soil thickness-dependent model results from variations in particle motions that vary with depth within the soil. In most soils, porosity decreases with depth and leads to an exponential-like porosity profile which results in an exponential particle velocity profile. In general, thicker soils will have a greater particle velocity near the surface and have larger depth-averaged velocities which leads to a soil-thickness dependency which can be approximated by (Furbish et al., 2009),

$$q_c = -D_n h(x) \frac{\partial \zeta}{\partial x}, \tag{2}$$

where D_{ch} [L T^{-1}] is another topographic diffusivity for creep-like processes but has different units than D_c and incorporates the depth-dependency of transport. Using either of these two alternatives to describe the flux will change the time evolution of pit-mound couplets. Numerical simulation of pit-mound couplets according to all three models demonstrates that, although they lead to slight differences in topographic evolution, the evolution of topographic variance follow similar paths.

3. Fitting Pit-Mound Couplets

We use high resolution DEMs with 0.25 m resolution to inform our parameters for pit-mound couplet geometry. An approximately 1 km^2 plot of land in south-central Indiana was scanned with a lidar-equipped UAV-drone. This particular site has over 600 mapped pit-mound couplets. We selected over 100 of these and fit the idealized geometry to them using a routine in Python which returned values for A, l, w, the orientation, and a squared difference between the observed and modeled. The average difference between observed and modeled is often less than 0.1 meters (Figure B1). In many cases, the amplitudes and dimensions of the couplets appear to match the natural couplets. However, the mismatch also includes the differences between the rough and potentially sloped ground outside of the couplet which contributes to the mismatch values.

4. Initial Pit-Mound Geometry We expect that the initial pit-mound couplet geometry varies with slope because, on steeper slopes, more sediment is deposited downslope of the pit. This will lengthen the couplet, and l should be longer on steeper slopes. We have created a simple one-dimensional model that simulates the initial uprooting and deposition of sediment on hillslopes with different steepness. The model treats a root mass as a one-dimensional rectangle that gets uprooted so that the long axis is perpendicular to the land-surface. This mass of sediment is then virtually dropped to the land-surface which creates an angular profile of a pit-mound couplet, which has unrealistic slopes (Figure S4a). The model numerically diffuses the angular pit-mound couplet until the maximum slope is below a critical slope. In this case, we have set a critical slope of 1. Running this model on couplets formed on different slopes produces pit-mount couplet geometries that vary with land-surface slope (Figure S4b). In particular, there is a nonlinear relationship between the length-scale of couplet geometries and land-surface slope (Figure S4c). We simplify this relationship and assume a linear relationship as most slopes in southern Indiana are below 0.6.

Data Table of measured R values by direction and the number of hillslopes measured.

Aspect	R	**# hillslopes**
North	0.18	292
Northeast	0.22	410
East	0.22	463
Southeast	0.19	189
South	0.19	63
Southwest	0.16	100
West	0.14	163
Northwest	0.17	231

References

Furbish, D. J., Haff, P. K., Dietrich, W. E., & Heimsath, A. M. (2009). Statistical description of slope-dependent soil transport and the diffusion-like coefficient. *Journal of Geophysical Research*, *114*, F00A05. doi: 10.1029/2009JF001267

Lewis, Q. W., Edmonds, D. A., & Yanites, B. J. (2020). Integrated uas and lidar reveals the importance of land cover and flood magnitude on the formation of incipient chute holes and chute cutoff development. *Earth Surface Processes and Landforms*, *45*(6), 1441–1455.

Mudd, S. M., & Furbish, D. J. (2004). Influence of chemical denudation on hillslope morphology: INFLUENCE OF CHEMICAL DENUDATION ON HILLSLOPES. *Journal of Geophysical Research: Earth Surface*, *109*(F2). doi: 10.1029/2003JF000087

Roering, J. J., Kirchner, J. W., & Dietrich, W. E. (2001). Hillslope evolution by nonlinear, slope-dependent transport: Steady state morphology and equilibrium adjustment timescales. *Journal of Geophysical Research: Solid Earth*, *106*(B8), 16499–16513. doi: 10.1029/2001JB000323

Roering, J. J., Perron, J. T., & Kirchner, J. W. (2007). Functional relationships between denudation and hillslope form and relief. *Earth and Planetary Science Letters*, *264*(1-2), 245–258. doi: 10.1016/j.epsl.2007.09.035

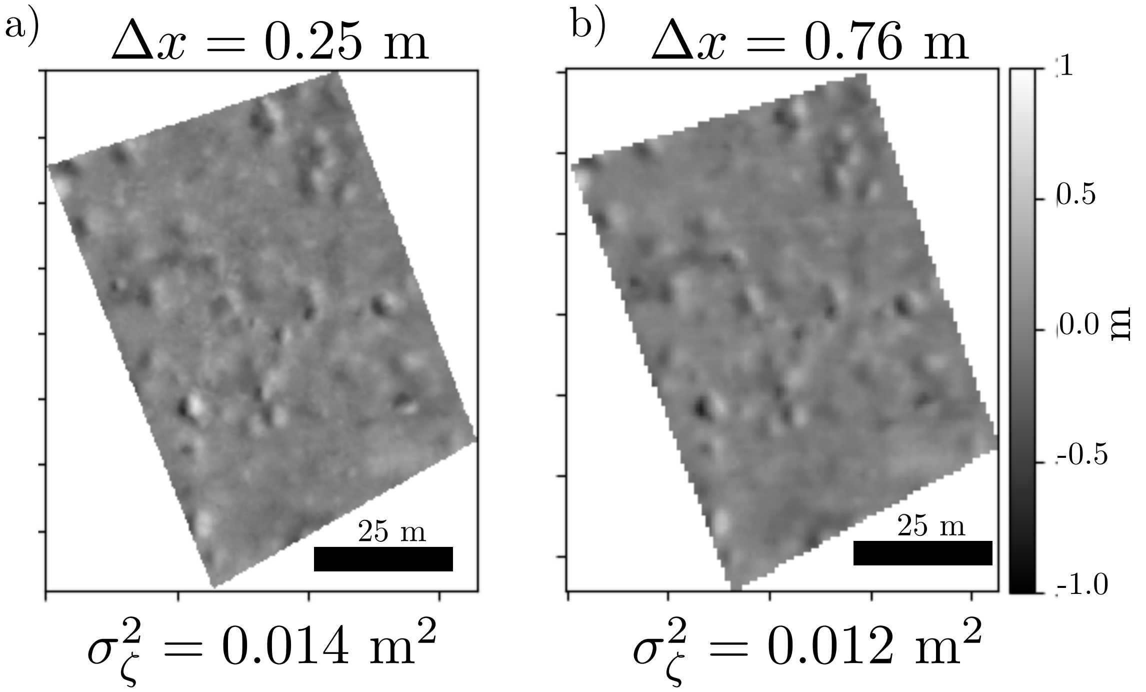

Figure S1. High pass filter of topography of a hillslope in Washington County, IN from 0.25-m (a) and 0.76-m (b) resolution data. The same pit-mound couplets are clearly visible in both datasets and measured variance values are similar.

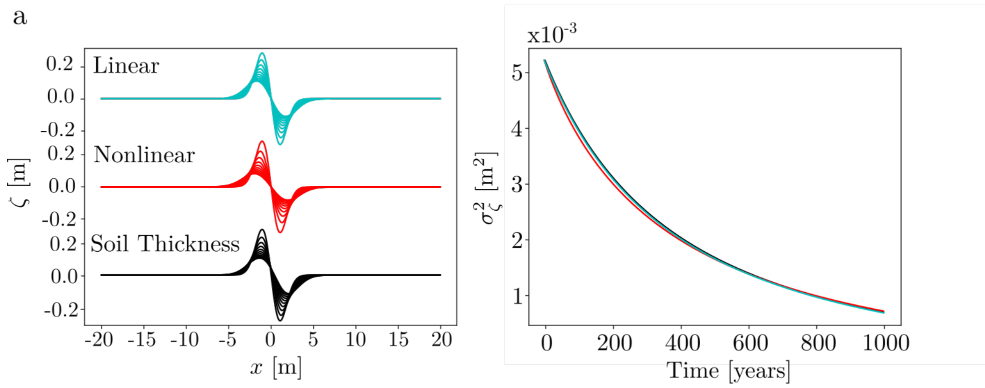

Figure S2. (a) Topographic evolution of a pit-mound couplet according to linear, nonlinear, and soil thickness-dependent transport models. Pit-mound couplets were originally on a background slope of 0.4 and we have used S_c=1.2 and μ_h=1 m (b) Time evolution of topographic variance of pit mound couplets according to all three models. The choice of model is apparently relatively unimportant for the time-series of topographic variance of pit-mound couplets.

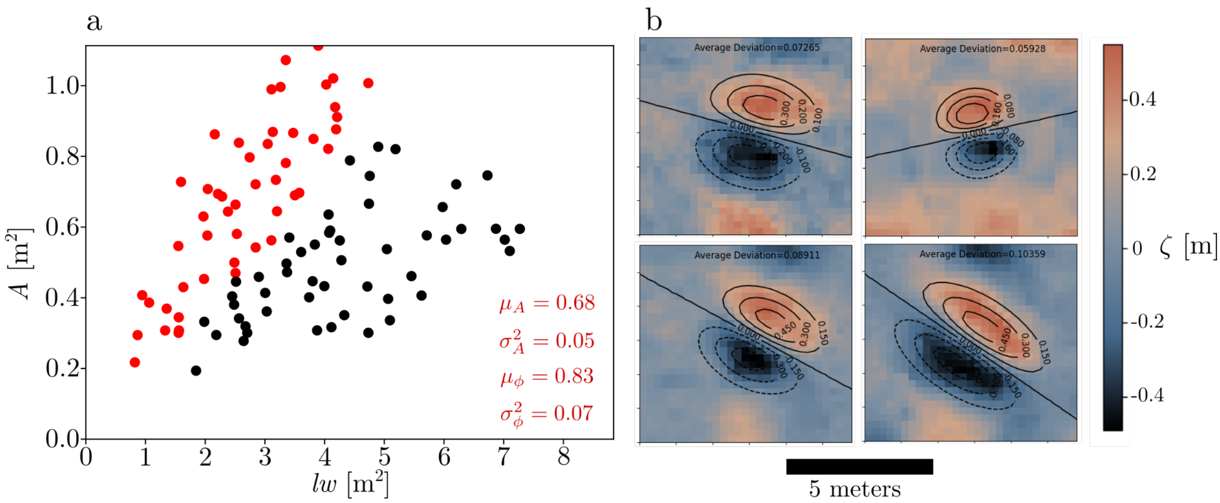

Figure S3. (a) Parameters extracted from 101 couplets from 0.25 m resolution lidar. Red dots are identified as the freshest as the 50 highest values of A/lw. (b) Four examples of natural couplets (colored surface) and the fit couplet (contours) with average deviation over the domain recorded in the top of the image.

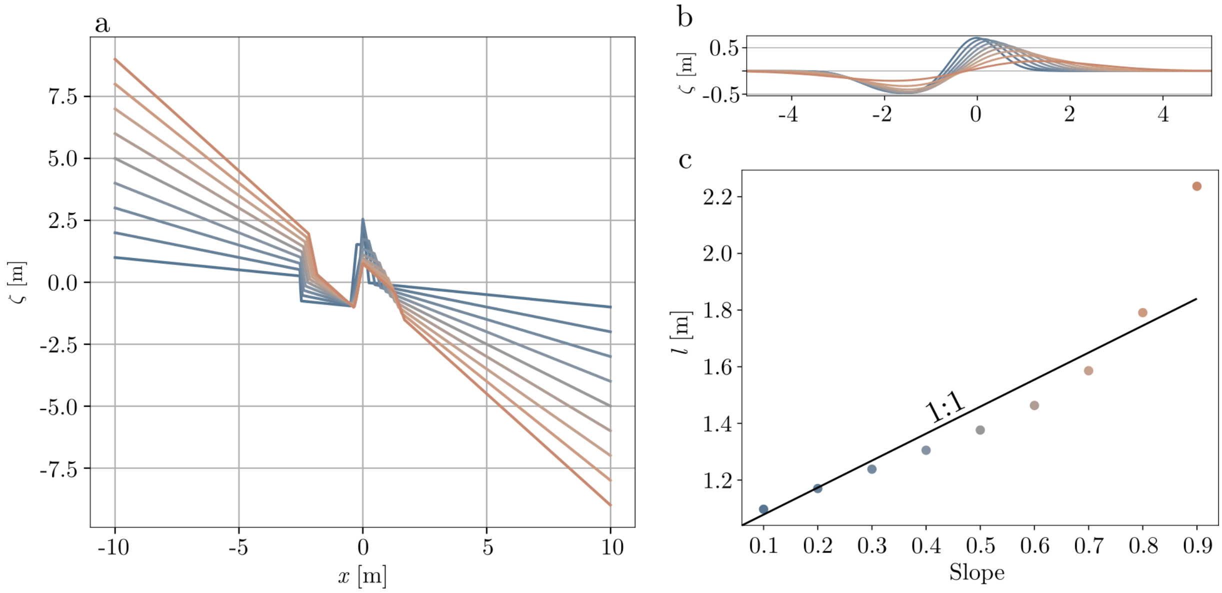

Figure S4. a) One dimensional model of an initial pit-mound couplet where a rectangle is uprooted perpendicular to the slope and all mass is dropped straight down on different slopes. On steeper slopes, more sediment falls downslope of the pit. b) Initial conditions of pit-mound couplets when we diffuse the profiles in (a) until a threshold slope is met - which is 1 in this case. c) Length-scale of the idealized pit-mound couplet that best fits the initial conditions in (b).